CrossMark

# Evolving LMXBs: CARB Magnetic Braking

Kenny X. Van and Natalia Ivanova

Department of Physics, University of Alberta, Edmonton, AB T6G 2E7, Canada; kvan@ualberta.ca

## Abstract

The formation of low-mass X-ray binaries (LMXBs) is an ongoing challenge in stellar evolution. An important subset of LMXBs is the binary systems with a neutron star (NS) accretor. In NS LMXBs with nondegenerate donors, the mass transfer (MT) is mainly driven by magnetic braking (MB). The discrepancies between the observed MT rates and the theoretical models were known for a while. Theory predictions of the MT rates are too weak and differ by an order of magnitude or more. Recently, we showed that with the standard MB, it is not possible to find progenitor binary systems such that they could reproduce—at any time of their evolution—most of the observed persistent NS LMXBs. In this Letter we present a modified MB prescription, Convection And Rotation Boosted (CARB). CARB MB combines two recent improvements in understanding stellar magnetic fields and magnetized winds—the dependence of the magnetic field strength on the outer convective zone and the dependence of the Alfvèn radius on the donor's rotation. Using this new MB prescription, we can reproduce the observed MT rates at the detected mass ratio and orbital period for all well-observed to-the-date Galactic persistent NS LMXBs. For the systems where the effective temperature of the donor stars is known, theory agrees with observations as well.

*Unified Astronomy Thesaurus concepts:* Binary stars (154); Stellar evolution (1599); Stellar evolutionary models (2046)

## 1. Introduction

Understanding the evolution of stars in binary systems relies heavily on the adopted laws of angular momentum loss that affect the change in orbital separation. One of the ways to lose angular momentum in a binary system is through magnetic braking (MB; Verbunt & Zwaan 1981). In this concept, the donor loses its angular momentum through a magnetized wind, and then, through tidal friction, replenishes the donor's angular momentum using the orbital angular momentum. MB is the dominant angular momentum loss mechanism in binaries wider than a few hours in orbital period, whereas gravitational radiation dominates in close binaries (Rappaport et al. 1983). More recently, circumbinary disks have been shown to effectively remove angular momentum and reproduce ultra-compact X-ray binaries (UCXBs; Ma & Li 2009a). Unfortunately, circumbinary disks appear to be rare in low-mass X-ray binaries (LMXBs) and there are significant uncertainties in the disk parameters (Ma & Li 2009a). Additionally, our work includes systems with wider periods that UCXBs. As such, we will be focusing only on MB.

The choice of the adopted MB prescription has large overarching effects on the evolution of the binary—stronger MB will shrink a binary faster, resulting in a higher mass transfer (MT) rate. The most widely used assumption in stellar simulations is the "Skumanich" MB (Skumanich 1972); its application to binary systems is usually the form provided in Rappaport et al. (1983). The standard MB law, as well as some of its modifications, fails to reproduce the observed persistent neutron star (NS) LMXBs (Van et al. 2019). Examples of some modified MB schemes include those which focus on a subset of LMXBs such as Ap/Bp donors (Justham et al. 2006), or dampen the MB strength at high rotation rates (Sills et al. 2000; Ivanova & Taam 2003).

Some advances in understanding the characteristics of the magnetized wind from a star were made recently. First, Réville

et al. (2015) have included the effect of stellar rotation on the Alfvèn radius. Second, the convective turnover time has been linked to the strength of the surface magnetic field (Parker 1971; Noyes et al. 1984; Ivanova 2006). In Section 2, we derive the new Convection And Rotation Boosted (CARB) MB that takes into account both advances. In Section 3, we use the new MB to evolve the grid of progenitor binaries, in a similar manner as done in Van et al. (2019). In Section 4, we compare the results of the simulations with the observed persistent NS LMXBs. Finally, in Section 5 we summarize our key results in this Letter.

## 2. Magnetic Braking

The loss of the angular momentum due to MB is derived following steps similar to those outlined in Van et al. (2019).

First, we assume spherical symmetry, which results in the angular momentum lost being

$$\dot{J}_{MB} = -\frac{2}{3}\Omega\dot{M}_W R_A^2. \qquad (1)$$

$\dot{M}_W$ denotes the wind mass-loss rate, $\Omega$ is the rotation rate, and $R_A$ is the Alfvèn radius. Assuming a radial magnetic field,

$$\left(\frac{R_A}{R}\right)^2 = \frac{B_s^2 R^2}{4\pi R_A^2 \rho_A v_A^2} = \frac{B_s^2 R^2}{\dot{M}_W v_A}. \qquad (2)$$

Here $R$ is the radius of the star, $B_s$ is the surface magnetic field strength, $v_A$ is the Alfvèn velocity, and $\rho_A$ is the density of the wind at the Alfvèn radius. Total mass loss with the wind is $\dot{M}_W = 4\pi R_A^2 \rho_A v_A$. The velocity of a normal stellar wind, when it reaches the Alfvèn radius, can be found from energy conservation, and expressed using the surface escape velocity

$v_{\rm esc}$:

$$\frac{v_{\rm A}}{v_{\rm esc}} = \left(\frac{R}{R_{\rm A}}\right)^{1/2}. \qquad (3)$$

In the case when the star and its attached magnetic field rotate, the regular stellar wind can also be additionally accelerated by the time it reaches the Alfvèn radius. This acceleration was tested by Matt et al. (2012) and was shown to have a nonnegligible effect. Réville et al. (2015) parameterized the additional acceleration by replacing the surface escape velocity with a modified velocity, which includes the effects of rotation. Using this variable instead in Equation (2) gives us

$$\left(\frac{R_{\rm A}}{R}\right)^3 = \frac{B_s^4 R^4}{\dot{M}_{\rm W}^2} \times \frac{1}{v_{\rm esc}^2 + 2\Omega^2 R^2/K_2^2}, \qquad (4)$$

where $K_2 = 0.07$ in this equation is a constant obtained from a grid of simulations by Réville et al. (2015). $K_2$ sets the limit where the rotation rate begins to play a significant role. In this approach, the Alfvèn radius shrinks as the rotation rate increases, weakening the angular momentum loss in fast rotating binaries. Plugging this form of the Alfvèn radius into the angular momentum equation gives a new prescription for angular momentum loss,

$$\dot{J}_{\rm MB} = -\frac{2}{3}\Omega\dot{M}_{\rm W}^{1/3}R^{14/3}B_s^{8/3}(v_{\rm esc}^2 + 2\Omega^2 R^2/K_2^2)^{-2/3}. \qquad (5)$$

Substituting a convective turnover scaling relation for the magnetic field strength of the star (see Van et al. 2019 for a discussion as to why this is justified), we get the modified MB prescription used in our simulations,

$$\dot{J}_{\rm MB} = -\frac{2}{3}\dot{M}_{\rm W}^{1/3}R^{14/3}(v_{\rm esc}^2 + 2\Omega^2 R^2/K_2^2)^{-2/3}$$
$$\times \Omega_\odot B_\odot^{8/3}\left(\frac{\Omega}{\Omega_\odot}\right)^{11/3}\left(\frac{\tau_{\rm conv}}{\tau_{\odot,\rm conv}}\right)^{8/3}. \qquad (6)$$

The magnetic field strength on the surface of the Sun is on average $B_s = 1$ G with a rotation rate and convective turnover time of $\Omega_\odot \approx 3 \times 10^{-6}$ s$^{-1}$ and $\tau_{\odot,\rm conv} = 2.8 \times 10^6$ s, respectively. Both solar values used here were found using the same method from Van et al. (2019). The value used for $\tau_{\odot,\rm conv}$ is similar to those found by Ma & Li (2009b) and Landin et al. (2010) of 28.4 days and 38.2 days, respectively. While our value deviates slightly from those found in other works, what is important is that our calculations are self-similar between different stars: the method used to calculate the normalization factor and the turnover time of each of our simulated systems is the same.

## 3. Evolution through the MT

We follow the method described in Van et al. (2019) and test the MB on progenitor binaries seeded on a grid of periods and donor masses. The initial periods range from $-0.4 \leqslant \log_{10}(P/{\rm day}) \leqslant 4$ in steps of $\Delta \log_{10}(P) = 0.05$. The initial donor masses range from $1.0 \leqslant M_d/M_\odot \leqslant 7.0$ with a variable step size. The donor mass has steps of $\Delta M_d = 0.1\,M_\odot$ when $M_d \leqslant 2.4 M_\odot$, $\Delta M_d = 0.2 M_\odot$ for $2.4 < M_d/M_\odot \leqslant 3$, $\Delta M_d = 0.5 M_\odot$ when $3 < M_d/M_\odot \leqslant 5$ and $\Delta M_d = 1.0 M_\odot$ for

any initial donor mass exceeding $5\,M_\odot$. The stars have initial metallicity $Z = 0.02$. All NSs start with a seed mass of $M_{\rm NS} = 1.4 M_\odot$. The chosen grid encompasses all binaries that could start the MT at some point of their evolution.

To evolve the initial binaries, we use the stellar code Modules for Experiments in Stellar Astrophysics (MESA[1]) revision 11701 (Paxton et al. 2011, 2013, 2015, 2018, 2019) and the 2019 May release of MESASDK.[2,3]

Here, we refine the method described in Van et al. (2019) by taking into account the efficiency of the MT. The rate of the mass gain of the NS $\dot{M}_{\rm NS}$ is proportional to the rate of the mass accretion $\dot{M}_{\rm acc}$, but is less than that due to conversion of some accreted mass into gravitational binding energy:

$$\dot{M}_{\rm NS} = \dot{M}_{\rm acc} f_{\rm BE}. \qquad (7)$$

Here $f_{\rm BE}$ is the so-called binding energy factor. Depending on the equation of the state of the NS, $f_{\rm BE} \approx 0.85$–$0.90$ (Lattimer & Prakash 2007). Some fraction of the material accreted onto the NS will be converted to gravitational binding energy and is controlled by $f_{\rm BE}$.

In addition, not all mass transferred through $L_1$ has to be accreted by the NS—it may be reduced by a number of effects, for example, the propeller effect is a mechanism where the magnetic field deflects away accreting material (Romanova et al. 2018). Indirect evidence for the accretion inefficiency comes from observations of millisecond pulsars. If the accretion rate was the same as the MT rate $\dot{M}_{\rm tr}$, many of these binaries are expected to contain high-mass neutron stars. However, the observations do not support this (Antoniadis et al. 2012, 2016). An analytic description of the efficiency of MT is not currently known. Antoniadis et al. (2012) calculated that accretion onto the pulsar PSR J1738+0333 had an efficiency $\epsilon \sim 0.1$–$0.3$, while a more recent statistical study looking at a number of pulsars estimated that their accretion efficiency was between $\epsilon \sim 0.05$ and $0.2$ (Antoniadis et al. 2016). We will combine the efficiency and the binding energy factor into one value $\eta$. The material accreted by the NS is less than that transferred,

$$\dot{M}_{\rm acc} = \eta\dot{M}_{\rm tr}. \qquad (8)$$

In Figure 1 we demonstrate how the choice of $\eta$ affects the mass of the final NSs. With $\eta = 1$, NSs in most systems become more massive than $2M_\odot$, once $M_d < 0.4 M_\odot$. While $M_{\rm NS}$ is predicted to extend up to $\approx 2.1$–$2.2 M_\odot$ no NSs have accurately and reliably measured masses exceeding $2.0 M_\odot$ (Antoniadis et al. 2013; Rezzolla et al. 2018; Cromartie et al. 2019). The rarity of high-mass NSs appears to contradict our results when assuming high efficiency. With $\eta = 0.2$, the maximum mass of the NS is of order $M_{\rm NS} \sim 1.8 M_\odot$. This value is within the range of $1.1 \lesssim M_{\rm NS}/M_\odot \lesssim 2$ for observed NSs (Özel & Freire 2016). For our study in this Letter, we therefore adopt $\eta = 0.2$.

The efficiency factor will have a variety of effects on the binary system. The increased mass ejected from the system will increase the amount of angular momentum lost and limit how quickly $M_{\rm NS}$ grows. The efficiency controls how much material is accreted onto the compact object, which sets the luminosity
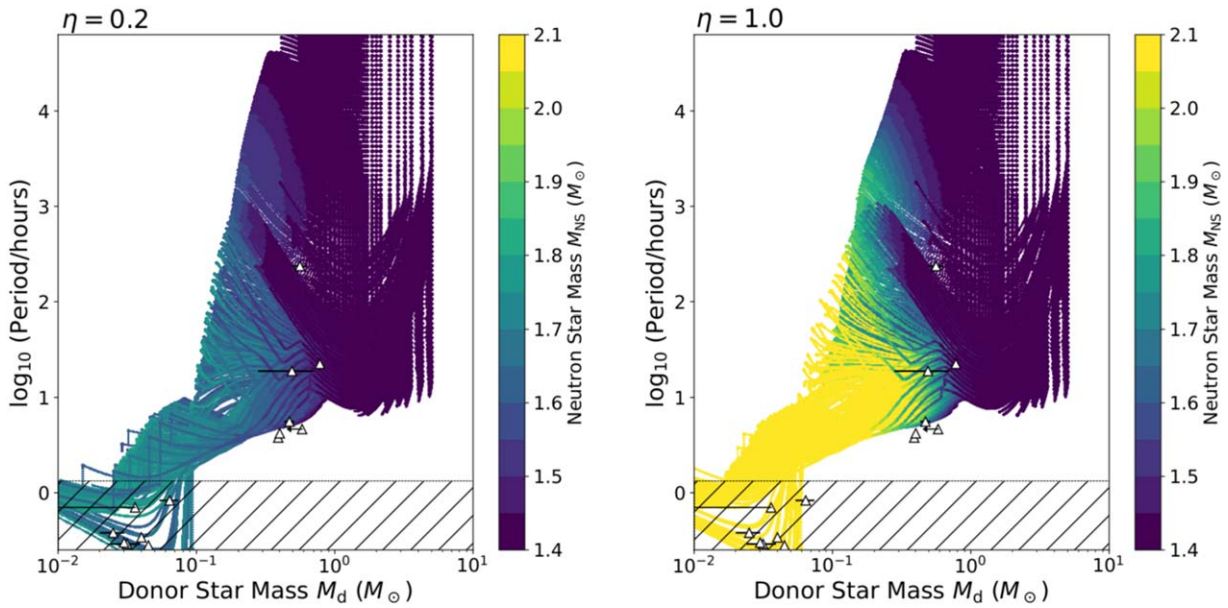
---

**Figure 1.** Evolution of $M_{NS}$ during the mass transfer. The $\eta$ value denotes the MT efficiency. The triangle symbols represent persistent LMXBs (data from Van et al. 2019).

of the system. The MT efficiency is not constant throughout the entire evolution, and as a rough approximation we will estimate that the luminosity of our system can be approximated by $L = 0.6 G \dot{M}_{tr} M_{NS}/R_{NS}$. We increase the size of our MT bins used in the analysis to compensate for the uncertainty in MT efficiency. If the $\eta$ parameter used here were applied to the results from Van et al. (2019), the overall ability of a system to reproduce an observed LMXB would remain unchanged or decrease as the MT rate required to explain the observed X-ray luminosity may be increased.

### 4. Comparison with the Observed Population of LMXBs

It has been shown that the results of the MT simulations can be misleading in determining the legitimacy of adopted MB prescriptions if only two parameters are compared between simulated and observed systems (Pavlovskii & Ivanova 2016). At least three parameters—for example, the period, the MT rate, and the mass ratio—are necessary for determining if a given MB prescription is effective. The effective temperature of the donor could also play a significant role in discriminating the adopted MB laws (Justham et al. 2006).

It is hard to visualize the compatibility of three or more parameters in the same figure. In Figure 2, we show the maximum relative probability for any of the simulated MT systems to have a specific MT rate and orbital period, as well as the MT rates and orbital periods of observed persistent NS LMXBs (data are taken from Van et al. 2019). This relative probability, or frequency, is calculated using the following steps:

1. $\tau_{tot}^{mn}$ is the total evolutionary time of a binary system for an initial mass $m$ and initial period $n$.
2. $\tau_{ij}^{mn}$ is the amount of time the initial $m$, $n$ binary spends in an observed $i$, $j$ period and MT bin.
3. $f_{ij}^{mn} = \tau_{ij}^{mn}/\tau_{tot}^{mn}$ is the frequency with which a given combination of mass and period appears in an observed bin of interest.
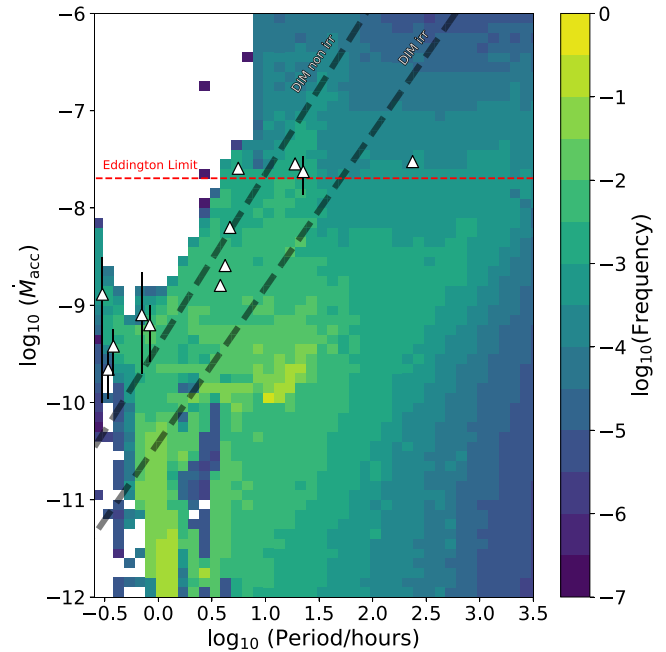


**Figure 2.** Relative probability of finding a system in a given bin in period–MT space. Each bin spans a width and height of 0.1 in $\log_{10}(P)$ and $\log_{10}(\dot{M}_{acc})$. The symbols used are the same as in Figure 1. The two gray dashed lines represent the critical MT separating persistent and transient systems for $M_{NS} = 1.4 \, M_{\odot}$ as described by the disk instability model (DIM; Coriat et al. 2012). The upper line includes the effects of irradiation while the lower line does not.

4. $f_{ij} = \max (f_{ij}^{mn})$ is the maximum frequency from all the simulated binaries, and is plotted in Figure 2.

Within this period–MT parameter space, all of the observed persistent NS LMXBs appear to be reproducible by the simulated MT systems. This apparent match does not guarantee that the simulated systems will reproduce the observed systems when additional parameters are included.

**Table 1**
Binned Properties of LMXBs

| System Name | $\log_{10}(P/\text{hr})$ | q | $\log_{10}(\dot{M}_a)$ | $\tau_{\max}$ (yr) | $A_{\text{sys}}/A_{\text{tot}}$ | $f_{\text{LMXB}}$ |
|---|---|---|---|---|---|---|
| 4U 0513-40 | [−0.57, −0.52] | [0.01, 0.06] | [−9.0, −8.4] | $5.87 \times 10^6$ | $1.72 \times 10^{-3}$ | $4.38 \times 10^{-2}$ |
| 2S 0918-549 | [−0.56, −0.51] | [0.01, 0.06] | [−9.6, −8.4] | $5.63 \times 10^6$ | $1.72 \times 10^{-3}$ | $4.38 \times 10^{-2}$ |
| 4U 1543-624 | [−0.54, −0.49] | [0.01, 0.06] | [−8.9, −8.4] | $5.85 \times 10^6$ | $1.54 \times 10^{-3}$ | $4.38 \times 10^{-2}$ |
| 4U 1850-087 | [−0.48, −0.43] | [0.01, 0.06] | [−9.8, −8.2] | $1.58 \times 10^7$ | $2.92 \times 10^{-3}$ | $8.82 \times 10^{-2}$ |
| M15 X-2 | [−0.44, −0.39] | [0.01, 0.06] | [−9.5, −8.9] | $2.43 \times 10^7$ | $2.92 \times 10^{-3}$ | $5.37 \times 10^{-2}$ |
| 4U 1626-67 | [−0.17, −0.12] | [0.01, 0.06] | [−9.5, −8.4] | $7.39 \times 10^7$ | $2.92 \times 10^{-3}$ | $1.05 \times 10^{-1}$ |
| 4U 1916-053 | [−0.10, −0.05] | [0.03, 0.08] | [−9.4, −8.7] | $6.14 \times 10^7$ | $1.03 \times 10^{-3}$ | $8.86 \times 10^{-2}$ |
| 4U 1636-536 | [0.56, 0.61] | [0.15, 0.40] | [−8.9, −8.4] | $2.32 \times 10^7$ | $5.49 \times 10^{-3}$ | $5.85 \times 10^{-2}$ |
| GX 9+9 | [0.60, 0.65] | [0.20, 0.33] | [−8.5, −8.0] | $1.39 \times 10^7$ | $4.46 \times 10^{-3}$ | $9.11 \times 10^{-2}$ |
| 4U 1735-444 | [0.65, 0.70] | [0.29, 0.48] | [−8.2, −7.7] | $1.11 \times 10^7$ | $4.97 \times 10^{-3}$ | $1.44 \times 10^{-2}$ |
| 2A 1822-371 | [0.73, 0.78] | [0.26, 0.36] | [−7.6, −7.1] | $5.95 \times 10^6$ | $6.69 \times 10^{-3}$ | $7.06 \times 10^{-2}$ |
| Sco X-1 | [1.26, 1.31] | [0.15, 0.58] | [−7.8, −7.1] | $5.42 \times 10^6$ | $1.20 \times 10^{-3}$ | $4.32 \times 10^{-3}$ |
| GX 349+2 | [1.33, 1.38] | [0.39, 0.65] | [−7.8, −7.1] | $1.21 \times 10^7$ | $4.46 \times 10^{-3}$ | $4.25 \times 10^{-3}$ |
| Cyg X-2 | [2.35, 2.40] | [0.25, 0.53] | [−7.5, −7.0] | $7.99 \times 10^4$ | $1.72 \times 10^{-3}$ | $6.65 \times 10^{-4}$ |

**Note.** The binned properties of observed persistent NS LMXBs taken from Van et al. (2019). This table is adapted from Table 4 of Van et al. (2019). Again the periods are in hours and the mass accretion rate $\dot{M}_a$ is in $M_\odot \text{yr}^{-1}$. The bin ranges were chosen to span the errors in the given observed property with the bins centered on the observed values. $\tau_{\max}$ is the maximum amount of time a given simulated system spends in the observed bin of interest. $A_{\text{sys}}/A_{\text{tot}}$ is the fraction of our tested parameter space that can reproduce the system of interest. These two quantities give an indication to how long a simulation appears similar to an observed LMXB and how many systems could reproduce these properties.

Let us briefly describe the methodology for the comparison in three-parameter space (for details, see Van et al. 2019). Each observed system is assigned a three-dimensional cuboid, where the cuboid is roughly centered in the observed properties. The size of of the cuboid in period is $\delta \log_{10} P = 0.05$, and the size of the cuboid in mass ratio and MT rate depend on the uncertainty with which the observed value was determined; see Table 1.

We can find the maximum time that an individual simulation spends in a bin of interest, $\tau_{\max}$, and what fraction of their MT evolution they spend in the given bin, $f_{\text{LMXB}}$. We also can find the fractional area of the initial parameter space that reproduces the binary $A_{\text{sys}}/A_{\text{tot}}$. These three numbers can indicate how plausible it is to produce the observed NS LMXBs. The value of $\tau_{\max}$ indicates how long a system can remain in this state, and thus how likely it is to be detected. $A_{\text{sys}}/A_{\text{tot}}$ shows how stringent the initial parameter space is for reproducing a given LMXB. A larger $A_{\text{sys}}/A_{\text{tot}}$ implies that many systems can reproduce an observed system. $A_{\text{tot}}$ spans our entire parameter space of seed masses and periods. In our case $A_{\text{tot}} = 29.1475$. For example, we find that Cyg X-2 only has two progenitor systems, these two progenitor systems span a total area of $A_{\text{sys}} = 0.05$, which results in $A_{\text{sys}}/A_{\text{tot}} = 1.72 \times 10^{-3}$.

As has been shown by Van et al. (2019), once the constraint on the mass ratio is added, none of the previously used MB prescriptions can produce all of the observed persistent NS LMXBs, despite considering all possible initial binaries. For the nonreproducible systems, $A_{\text{sys}}/A_{\text{tot}} = 0$. In Table 1 we present the results for the CARB MB prescription. It is fascinating that with the modified MB prescription, all persistent LMXBs can be reproduced.

We can further constrain the progenitors by looking at the effective temperature of the donor star. Determining the temperature of the companion is difficult, and this value is not known for most observed LMXBs. The systems where the donor's spectral type have been measured tend to be the widest LMXBs; Sco X-1, GX 349+2, and Cyg X-2. This additional fourth observed parameter will provide additional constraints to

the progenitor mass and period combinations that result in binaries that can match all observed properties.

Sco X-1 was found to have a donor star that was later than K4 (Mata Sánchez et al. 2015). This gives an approximate upper limit to the donor temperature to be $\lesssim 4800$ K. By matching our three previous properties of interest—period, mass ratio, and MT—while constraining the donor temperature, we can further limit systems that reproduce Sco X-1. An example progenitor of Sco X-1 has a $1.1\,M_\odot$ donor with an initial period of 2.82 days. This system simultaneously matches the period, mass ratio, MT, and effective temperature of Sco X-1. When this progenitor evolves to the observed mass ratio and period, the MT rate and effective temperature of the binary are $2.3 \times 10^8\,M_\odot\,\text{yr}^{-1}$ and 4685 K, respectively.

Cyg X-2 was found by Cowley et al. (1979) to have an A5-F2 donor star. A5-F2 spectral type stars have an approximate temperature range of 7000–8500 K. When comparing this to our MT systems, we find that the only progenitors that reproduce Cyg X-2 are binaries with an initial period between $P \approx 2.24$–2.51 days and an initial donor mass of $M = 3.5\,M_\odot$. The MT rates and effective temperatures of the 2.24 day progenitor are $2.9 \times 10^{-8}\,M_\odot\,\text{yr}^{-1}$ and 7265 K.

GX 349+2 is a system where the spectral class of the donor is given, but the literature related to this property is not in agreement. Penninx & Augusteijn (1991) found the donor of GX 349+2 to be a G5–M2 giant, whereas Wachter & Margon (1996) find the donor could be a B2 main-sequence donor. Our simulated results have a temperature ranging from $\approx 4800$–5500 K, which correspond to a K3–G5 donor star. An example progenitor of GX 349+2 is a binary with an initial donor mass of $M = 1.1\,M_\odot$ and a seed period of 3.98 days. This progenitor has an MT rate of $8.2 \times 10^{-8}\,M_\odot\,\text{yr}^{-1}$ and an effective temperature of 4845 K.

## 5. Conclusions

We revised the MB prescription to include the effect of the donor's rotation on the wind's velocity, following Matt et al. (2012) and Réville et al. (2015), as well as the effects of the donor's convective eddy turnover timescale and the donor's

rotation on the generation of the surface magnetic field, following Parker (1971), Noyes et al. (1984), Ivanova (2006), and Van et al. (2019).

The new CARB MB prescription was applied to test the evolution of all binaries with an NS and nondegenerate donors that could experience the MT at some point in their evolution. The modeled MT systems were compared to the observed persistent NS LMXBs. Our simulations were required to match with observations in three parameters—the MT rate, the orbital period, and the mass ratio, with the effective temperature being used as a fourth parameter in select binaries. Previously, it has been shown that the most commonly used MB prescription, also known as the Skumanich MB (Rappaport et al. 1983), is not capable of reproducing most of the persistent NS LMXBs with orbital periods longer than about an hour. With our modified MB, we can reproduce all observed persistent NS LMXBs.

We note that the "intermediate" prescription considered in Van et al. (2019) reproduced all of the LMXBs of interest as well, although that description was not explicitly derived—it was created by adding ad hoc wind boosting and ad hoc convection boosting. Both of these factors are taken into account in a more physical way in the modified MB prescription presented here. Additionally, once the effective temperature is accounted for with the "intermediate" prescription, Sco X-1 could no longer be reproduced. The number of possible progenitors of Cyg X-2 also significantly drops, to only one system.

Our simulations do not include additional effects such as irradiation, or atypically strong magnetic fields similar to those found in Ap stars. While these effects might be invoked to explain a specific individual system, they could not be used to explain the evolution of the entire population of MT binaries. The inclusion of rotational effects on the Alfvèn radius, and magnetic field dependence on convective turnover time, resulted in CARB MB being able to reproduce all of the observed persistent NS LMXBs. We unequivocally recommend the use of the CARB MB prescription, instead of the Skumanich MB, to model both Galactic and extragalactic NS LMXBs.

Once the governing angular momentum loss law is constrained, our next step will be to recover and constrain the properties of the plausible progenitor systems and the required formation rates of these progenitors to produce the observed numbers of LMXBs. We also intend to expand our sample size to include BHs and any additional well-constrained NSs available. This will be a topic of our future research.

### ORCID iDs

Kenny X. Van ⓘ https://orcid.org/0000-0003-3862-5826
Natalia Ivanova ⓘ https://orcid.org/0000-0001-6251-5315

### References

Antoniadis, J., Freire, P. C. C., Wex, N., et al. 2013, Sci, 340, 448
Antoniadis, J., Tauris, T. M., Ozel, F., et al. 2016, arXiv:1605.01665
Antoniadis, J., van Kerkwijk, M. H., Koester, D., et al. 2012, MNRAS, 423, 3316
Coriat, M., Fender, R. P., & Dubus, G. 2012, MNRAS, 424, 1991
Cowley, A. P., Crampton, D., & Hutchings, J. B. 1979, ApJ, 231, 539
Cromartie, H. T., Fonseca, E., Ransom, S. M., et al. 2019, NatAs, in press (doi:10.1038/s41550-019-0880-2)
Ivanova, N. 2006, ApJL, 653, L137
Ivanova, N., & Taam, R. E. 2003, ApJ, 599, 516
Justham, S., Rappaport, S., & Podsiadlowski, P. 2006, MNRAS, 366, 1415
Landin, N. R., Mendes, L. T. S., & Vaz, L. P. R. 2010, A&A, 510, A46
Lattimer, J. M., & Prakash, M. 2007, PhR, 442, 109
Ma, B., & Li, X.-D. 2009a, ApJ, 698, 1907
Ma, B., & Li, X.-D. 2009b, ApJ, 691, 1611
Mata Sánchez, D., Muñoz-Darias, T., Casares, J., et al. 2015, MNRAS, 449, L1
Matt, S. P., Pinzón, G., Greene, T. P., & Pudritz, R. E. 2012, ApJ, 745, 101
Noyes, R. W., Hartmann, L. W., Baliunas, S. L., Duncan, D. K., & Vaughan, A. H. 1984, ApJ, 279, 763
Özel, F., & Freire, P. 2016, ARA&A, 54, 401
Parker, E. N. 1971, ApJ, 164, 491
Pavlovskii, K., & Ivanova, N. 2016, MNRAS, 456, 263
Paxton, B., Bildsten, L., Dotter, A., et al. 2011, ApJS, 192, 3
Paxton, B., Cantiello, M., Arras, P., et al. 2013, ApJS, 208, 4
Paxton, B., Marchant, P., Schwab, J., et al. 2015, ApJS, 220, 15
Paxton, B., Schwab, J., Bauer, E. B., et al. 2018, ApJS, 234, 34
Paxton, B., Smolec, R., Schwab, J., et al. 2019, ApJS, 243, 10
Penninx, W., & Augusteijn, T. 1991, A&A, 246, L81
Rappaport, S., Verbunt, F., & Joss, P. C. 1983, ApJ, 275, 713
Réville, V., Brun, A. S., Matt, S. P., Strugarek, A., & Pinto, R. F. 2015, ApJ, 798, 116
Rezzolla, L., Most, E. R., & Weih, L. R. 2018, ApJ, 852, L25
Romanova, M. M., Blinova, A. A., Ustyugova, G. V., Koldoba, A. V., & Lovelace, R. V. E. 2018, NewA, 62, 94
Sills, A., Pinsonneault, M. H., & Terndrup, D. M. 2000, ApJ, 534, 335
Skumanich, A. 1972, ApJ, 171, 565
Van, K. X., Ivanova, N., & Heinke, C. O. 2019, MNRAS, 483, 5595
Verbunt, F., & Zwaan, C. 1981, A&A, 100, L7
Wachter, S., & Margon, B. 1996, AJ, 112, 2684